International Journal of Heat and Fluid Flow 30 (2009) 306–318

Contents lists available at ScienceDirect

International Journal of Heat and Fluid Flow

journal homepage: www.elsevier.com/locate/ijhff

Derivation of jump conditions for the turbulence $k-\epsilon$ model at a fluid/porous interface

M. Chandesris *, D. Jamet

Laboratoire de Modélisation et de Développement de Logiciels, DEN/DER/SSTH, CEA Grenoble, 17 rue des Martyrs, 38054 Grenoble Cedex 9, France

ARTICLE INFO

Article history:
Received 19 September 2007
Received in revised form 9 January 2009
Accepted 15 January 2009
Available online 23 February 2009

Keywords:
Turbulence modeling
$k-\epsilon$ model
Porous media
Boundary conditions
Interface
Excess quantity

ABSTRACT

The boundary conditions that must be imposed at a fluid/porous interface for the turbulence $k-\epsilon$ model is investigated in a two-step up-scaling framework, already introduced to study the laminar case [Chandesris, M., Jamet, D., 2006. Boundary conditions at a planar fluid–porous interface for a Poiseuille flow. Int. J. Heat Mass Transfer 49, 2137–2150]. The form of the momentum, $\langle k\rangle$ and $\langle\epsilon\rangle$ fluxes jump conditions are derived using a surface-excess theory of interfacial transport processes. These jump conditions are related to surface-excess quantities. These excess quantities are evaluated for a particular geometry of the porous medium for which DNS results are available [Breugem, W.P., Boersma, B.J., 2005. Direct numerical simulations of turbulent flow over a permeable wall using a direct and a continuum approach. Phys. Fluids 17 (2), 025103]. A very good agreement is obtained between the $k-\epsilon$ model and the DNS results. The study of this particular configuration also allows to show for the first time the validity of the macroscopic turbulent viscosity modeling for flows in porous media.

1. Introduction

This article deals with the computation of turbulent flows in a domain partially filled with a porous medium. The scientific domains concerned with these types of flows range from technological applications (packed-bed heat exchangers, nuclear waste repository, drying processes, etc) to environmental sciences (flows over plant canopies, flows in river, dispersion of pollutants over cities, etc).

There exists different approaches to compute such flows, depending mainly on the accuracy required for a given study compared to its computational cost. Breugem and Boersma (2005) and Breugem et al. (2006) performed direct numerical simulations (DNS) of turbulent channel flows over a 3D Cartesian grid of cubes where the cubes mimic a porous media. These computations give very comprehensive results and allow to gain more insight in the influence of the underlying porous layer on the dynamics and structure of the turbulence. However, they require an enormous computation power (between 10^7 and 10^8 grid points are needed) and therefore they cannot be used for practical analysis of engineering flows. Large eddy simulations (LES) allow to introduce a first level of modeling. These simulations are widely used to study turbulent flows over forests (Finnigan, 2000; Watanabe, 2004) mainly because they allow the capture of the unsteady character of the large eddies. However, these simulations still require a large computational power. For engineering studies where only the knowledge of the mean quantities is needed, turbulence $k-\epsilon$ models are more adequate. This approach, followed by many authors (Lee and Howell, 1987; De Lemos, 2005; De Lemos and Silva, 2006; Zhu and Kuznetsov, 2005; Uittenbogaard, 2003), requires the specification of $k-\epsilon$ models in the free fluid region and in the porous region, and then to connect these models at the fluid/porous interface. Turbulence $k-\epsilon$ models adapted to the porous region have been proposed in recent years (Nakayama and Kuwahara, 1999; Pedras and De Lemos, 2001a; Pinson et al., 2007; Chandesris et al., 2006). Indeed, the presence of the porous structure greatly affects the turbulence and the standard $k-\epsilon$ model is not valid in the porous region. Additional source terms, which account for the subfilter production and dissipation of k and ϵ due to the presence of the porous structure, are introduced. Different closures have been proposed for these additional terms, depending on the porous structure and also on the approach (Nakayama and Kuwahara, 1999; Pedras and De Lemos, 2001b). These macroscopic turbulence $k-\epsilon$ transport equations have been validated on different porous geometries. In particular, the additional source terms due to the subfilter production and dissipation of k and ϵ allow to correctly account for the evolution of the averaged turbulent kinetic energy and dissipation.

However, the physical configurations considered do not allow to validate the influence of k and ϵ on the velocity field via the macroscopic turbulent viscosity. Indeed, in these configurations, the gradient of the macroscopic velocity is zero and thus the turbulent viscosity has no effect on the velocity field. As a consequence, the

* Corresponding author.
E-mail address: marion.chandesris@cea.fr (M. Chandesris).

0142-727X/$ - see front matter © 2009 Elsevier Inc. All rights reserved.
doi:10.1016/j.ijheatfluidflow.2009.01.008

macroscopic turbulent viscosity obtained with these models has never been validated. Thus, the development and the validation of this type of model still need to be pursued using more complex configurations.

Thus, far from the fluid–porous interface, where the velocity gradients are negligible, the use of a macroscopic turbulence $k-\epsilon$ model is relevant. However, close to the interface, two issues arise. First, the velocity gradients are larger and the macroscopic turbulence $k-\epsilon$ model has to be validated (as stated above). Second, the specification of boundary conditions between the porous and free fluid $k-\epsilon$ models at the fluid/porous interface is still an open question. The physical configuration considered in this study allows to tackle these two issues.

Even for laminar flows, the specification of boundary conditions at a fluid/porous interface is not trivial and different boundary conditions are proposed in the literature (Beavers and Joseph, 1967; Neale and Nader, 1974; Ochoa-Tapia and Whitaker, 1995a). Neale and Nader (1974) suggest to impose continuity of both stress and velocity at the interface. However, Ochoa-Tapia and Whitaker (1995a,b) have shown that a discontinuity in the momentum diffusion flux can exist between the two media:

$$\left.\frac{d\langle u\rangle}{dy}\right|_{y=0^+} - \frac{1}{\phi_p}\left.\frac{d\langle u\rangle}{dy}\right|_{y=0^-} = -\frac{\beta}{\sqrt{K}}\langle u\rangle|_{y=0} \tag{1}$$

In this equation ϕ_p and K represent, respectively the porosity and the permeability of the porous medium, $\langle u\rangle$ is the *volume average* velocity and β is a jump coefficient.

Transposing these results to turbulent flows in hybrid fluid/porous domains, these different boundary conditions for the momentum equation have been tested (Lee and Howell, 1987; De Lemos and Pedras, 2000; Silva and De Lemos, 2003). In these studies, k, ϵ and their respective fluxes are supposed, without justification, to be continuous at the interface. More recently, De Lemos (2005) and De Lemos and Silva (2006) have tested a jump condition for the flux of the turbulent kinetic energy k, similar to the momentum jump condition proposed in (Ochoa-Tapia and Whitaker, 1995a):

$$\left(\mu+\frac{\mu_t}{\sigma_k}\right)\left.\frac{d\langle k\rangle}{dy}\right|_{y=0^+} - \left(\mu_{\text{eff}}+\frac{\mu_{t_\phi}}{\sigma_k}\right)\left.\frac{d\langle k\rangle}{dy}\right|_{y=0^-} = -(\mu+\mu_t)\frac{\beta}{\sqrt{K}}\langle k\rangle|_{y=0} \tag{2}$$

In this expression $\mu, \mu_{\text{eff}}, \mu_t$ and μ_{t_ϕ} represent, respectively the viscosity of the fluid, the effective viscosity of the porous medium, the turbulent viscosity and the macroscopic turbulent viscosity in the porous medium; σ_k is the Prandtl number associated to k and $\langle k\rangle$ is the *volume average* of k. Regarding the β coefficient, De Lemos and Silva (2006) acknowledge that a value different from the one used for the stress jump relation (1) might be necessary. However, the difficulty is to specify the value of this coefficient since its origin is unclear. It can be noticed that the same question holds regarding a possible jump for the flux of $\langle\epsilon\rangle$ at the interface.

The goal of this article is thus to derive in a coherent way the boundary conditions at a fluid/porous interface for the momentum, k and ϵ equations. Our objective is to gain more basic understanding about the form and the origin of these jump conditions. As a consequence, we should get more information about the value of the β coefficient of Eq. (2).

Following the work initiated by Ochoa-Tapia and Whitaker (1995a), Chandesris and Jamet (2006, 2007) have used a two-step up-scaling methodology to study the momentum transfer at a fluid/porous interface for laminar flows. This approach allows to get more insight about the origin of the stress jump condition which is related to surface-excess quantities. This approach also allows to make explicit the value of the jump coefficients depending on the location of the discontinuous interface and the structure of the porous medium. The idea is to pursue this approach and to transpose this methodology to the study of turbulent flows.

This article is organized as follows. After recalling the main ideas of the two-step up-scaling methodology, the first up-scaling step is performed. Then, in a second up-scaling step, the general forms of the fluxes jump conditions at the fluid/porous interface are derived. These jump conditions are shown to be related to excess quantities. The next section deals with the determination of these excess quantities for the particular geometry studied by Breugem and Boersma (2005). Finally, the macroscopic $k-\epsilon$ model is compared to the results of the DNS of Breugem and Boersma (2005).

2. Modeling approach

Ochoa-Tapia and Whitaker (1995a) introduced the idea of *deriving* the momentum boundary condition at a fluid/porous interface starting from the knowledge of the flow at the microscopic scale and using up-scaling methods. Formalizing this approach, Chandesris and Jamet (2006, 2007) have introduced three different levels of description of a fluid/porous interface: *microscopic*, *mesoscopic* and *macroscopic* (see Fig. 1).

At the *microscopic* scale, the flow in the entire fluid domain (free fluid region and pores of the porous medium) is governed by the well-known Navier–Stokes equations.

At the *mesoscopic* scale, the fluid and solid phases are replaced by a single equivalent continuous medium. At this level, the properties of the medium (e.g. porosity, permeability) are strongly but nevertheless continuously varying within a transition region that separates the homogeneous regions. The interface is diffuse.

Finally, at the *macroscopic* scale, the system consists in two homogeneous regions with constant properties, separated by a discontinuous, sharp interface. This scale of description is the most commonly used for the study of practical applications. However, it requires the specification of boundary conditions at the interface between the two homogeneous media.

The mesoscopic level is obtained by applying the filter used in the homogeneous porous region in the entire domain including the fluid–porous transition region. This region is thus transformed into a continuous transition zone across which all physical properties vary smoothly. This first up-scaling step goes from a microscopic level where the characteristic length is the size of the solid inclusions to another level, which we name the mesoscopic scale, where the fluid and solid phases are replaced by an effective medium. Its characteristic length is the scale of variation of the averaged quantities. This first up-scaling is associated to the *modeling of the porous medium*. However, since the same averaging volume is applied in the whole domain and in particular in the vicinity of the interface, this up-scaling step introduces a new characteristic length scale, the thickness δ of the interfacial transition region. This description is relevant to study transport phenomena on length scales of the order of δ.

The macroscopic level is relevant to study transport phenomena at length scales much larger than δ. Thus, at this scale it is useful to model the interface as an equivalent discontinuous surface, which allows to consider constant effective transport properties on both sides of the interface. Thus, the second up-scaling consists in replacing the diffuse interface of the mesoscopic level by an equivalent discontinuous surface. This second up-scaling is associated to the *modeling of the interface*. Thus, the mesoscopic and macroscopic models are the same in the homogeneous regions, but they are different in the interfacial transition region. In this regard, this second step is an up-scaling for the modeling of the fluid–porous interface.

The physical modeling of interfacial transfers occurs at the mesoscopic scale. Once this physical modeling has been performed, the

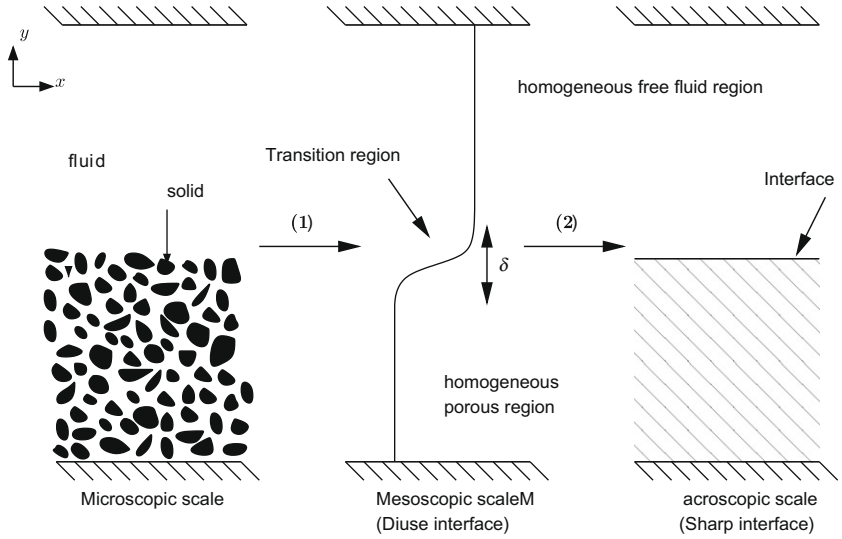

Fig. 1. The three different levels of description of a fluid/porous interface.

determination of the equivalent boundary conditions at the macroscopic discontinuous interface is rather a mathematical problem (Chandesris and Jamet, in press).

In Ochoa-Tapia and Whitaker (1995a) and Chandesris and Jamet (2006), the *first up-scaling step*, which allows to go from the microscopic to the mesoscopic description, is performed using the volume averaging method (Whitaker, 1999). The volume average operator is applied to the equations governing the flow at the microscopic scale in the entire domain. The obtained equations can be easily closed in the two homogeneous regions (free fluid and porous medium). However, the closure in the heterogeneous transition region is much more difficult, mostly because the length scale constraints that are necessary to simplify the closure problem are no longer valid in this region. The resolution of this complex closure problem is still the subject of on-going research, even for laminar flows. Since this problem is not solved yet, one way to overcome it is the following: (i) to postulate the form of the closed equation, (e.g. for laminar flows: the Darcy–Brinkman model with variable porosity and permeability profiles), (ii) from this closed form, to deduce the profiles of the parameters of the model in the transition region by filtering microscopic simulations (See for example the porosity and permeability profiles obtained in Breugem et al. (2004) and Chandesris and Jamet (2007)), (iii) to verify that these profiles are independent of the flow conditions. This verification ensures that the chosen model is indeed representative of the physic in the transition region. In this study, we will only postulate the form of the closed equations and study the consequences of this choice. We cannot validate the generality of the variable coefficients of the chosen model because not enough reference DNS results are available.

For the *second up-scaling step*, which allows to go from a diffuse to a discontinuous description of the interface, different methods can be used. It is worth noticing that this particular problem has been thoroughly studied for liquid/liquid, liquid/vapor and liquid/solid interfaces. Many different approaches have been suggested and the study of the fluid/porous interface could tremendously benefit from these. In particular, two techniques are worth being presented: the surface-excess theory of interfacial transport processes, presented in details by Edwards et al. (1991) and the method of matched asymptotic expansions (Zwillinger, 1989).

In the surface-excess theory of interfacial transport processes, generic conservation equations for the interfacial transports are derived by integrating the difference between the macroscopic and the mesoscopic equations governing the problem (see Edwards et al., 1991, Chapter 15). Indeed, by construction, the macroscopic equations are not suited to describe the flow in the transition region: they are valid only in the homogeneous regions. All the physical features that are accounted for in the mesoscopic model and not, or not correctly, in the macroscopic model are thus concentrated at the discontinuous interface by means of surface-excess quantities. We recall that for any physical field ψ, its excess quantity is defined by:

$$\psi^{EX} \hat{=} \int_{-\infty}^{y_M} (\psi(y) - \Psi_-)dy + \int_{y_M}^{+\infty} (\psi(y) - \Psi_+)dy \tag{3}$$

where y is the coordinate normal to the interface, y_M is the location of the discontinuous interface, ψ is the mesoscopic representation of the studied field, Ψ_- and Ψ_+ are the macroscopic representations of this field in the two homogeneous regions. When Ψ_- and Ψ_+ are constant, this relation can also be written:

$$\psi^{EX} = (y_i - y_M)(\Psi_- \Psi_+) + \int_{-\infty}^{y_i} (\psi(y) - \Psi_-)dy + \int_{y_i}^{+\infty} (\psi(y) - \Psi_+)dy \tag{4}$$

where y_i is any arbitrary position inside the transition region. This definition is illustrated in Fig. 2a, where the excess quantity is represented by the shaded area. It represents exactly the amount of the ψ field that is not seen by the macroscopic model in the interfacial transition region compared to the mesoscopic model. It should be noticed that with this definition, the value of the excess quantity depends on the choice of the position of the discontinuous interface y_M within the transition region. A particular position of the interface is the position such that the sum of the two integral terms of Eq. (3) is zero:

$$\int_{-\infty}^{y_\psi} (\psi(y) - \Psi_-)dy + \int_{y_\psi}^{+\infty} (\psi(y) - \Psi_+)dy = 0 \tag{5}$$

This particular position is noted y_ψ and is named the center of gravity of the profile of ψ. An illustration of this definition is given in Fig. 2b. Furthermore, using this definition, when Ψ_- and Ψ_+ are constant, the excess quantity can be simply expressed by:

$$\psi^{EX} = (y_\psi - y_M)(\Psi_- \Psi_+) \tag{6}$$

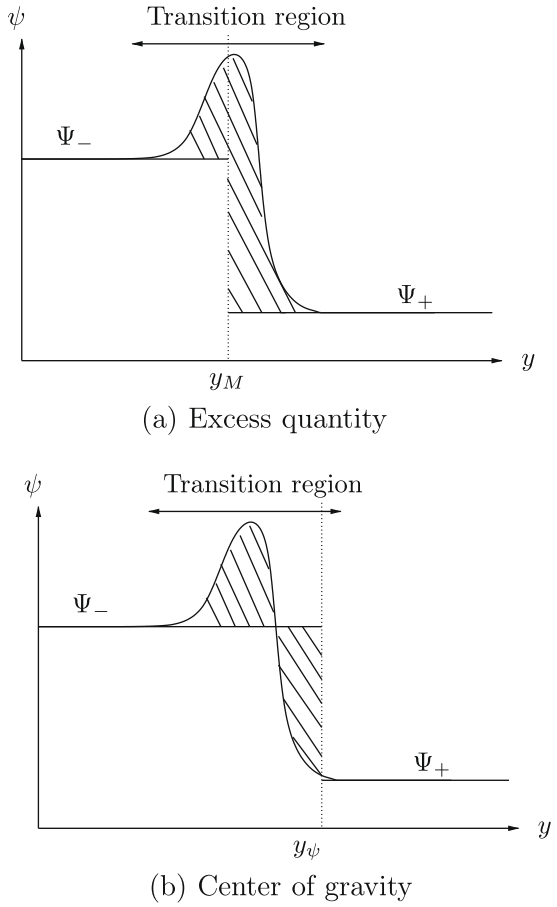

Fig. 2. Definition of an excess quantity.

The main advantage of the method presented by Edwards et al. (1991) is its generic character. The general *form* of the boundary conditions are determined relatively easily, even for three-dimensional problems. However, its major drawback is that the obtained boundary conditions are expressed through excess quantities of mesoscopic variables of the problem, which are *unknown* at the macroscopic level. Thus, these boundary conditions are not closed and an additional modeling or evaluation of these excess quantities is required to determine the value of the jump coefficients.

The idea of the second method, the method of matched asymptotic expansions, is to solve analytically, using an asymptotic expansion in ε, the equations governing the problem at the mesocopic scale. This asymptotic expansion is feasible because a small parameter, $\varepsilon = \delta/h$, is usually present in the mesoscopic equations. In our particular problem, δ is the size of the heterogeneous transition region and h is the height of the free fluid region. As ε tends to zero, the transition region tends to a discontinuous surface. Thus, this method allows to derive analytically, and at a given order, boundary conditions at an interface. Much physical information can be extracted from the results obtained with this method: Chandesris and Jamet (2007) were able to determine the value of the jump coefficients for laminar flows and to make explicit their dependence on the location of the discontinuous interface and on the structure of the porous medium. However, this analytical method can become very complex for three-dimensional or non-linear problems.

In this article, we will take advantage of the simplicity of the first method to derive the general form of the boundary conditions that must be applied for the $k-\epsilon$ model. Therefore, a simple modeling approach will be proposed to close the model. However, we acknowledge that this work could be deepened by the use of the second method, which is however much more technical. The two-step up-scaling methodology that we will use in this article is summarized in Fig. 3. We recall that the problem of the turbulence modeling is supposed to be solved *at the microscopic scale* by the use of the standard $k-\epsilon$ model (Launder and Spalding, 1972).

3. First up-scaling step

In order to derive a macroscopic turbulence model for flows in porous media, authors like Nakayama and Kuwahara (1999) apply the volume average operator to the $k-\epsilon$ model governing the problem at the microscopic scale. Thus, they are able to derive macroscopic transport equations for $\langle k\rangle$ and $\langle\epsilon\rangle$ in the homogeneous porous medium. To perform the first up-scaling step, the idea is to go further and to apply the volume average operator to the mass, momentum, k and ϵ transport equations *in the entire domain*, i.e. in the homogeneous porous region, in the transition region and in the homogeneous free fluid region. Following the ideas of the volume averaging theory (Whitaker, 1999), the filtered equations can be rearranged using the theorems of local volumetric averages (Slattery, 1972; Whitaker, 1969) and introducing the Gray's decomposition (Gray, 1975):

$$\psi = \langle\psi\rangle_f + \tilde{\psi} \tag{7}$$

where $\langle\psi\rangle_f$ denotes the *intrinsic volume average* of ψ and $\tilde{\psi}$ the deviation of the quantity ψ from its intrinsic volume average. At the end, the system is similar to the one presented in (Chandesris et al., 2006):

$$\nabla\cdot(\phi\langle\overline{\mathbf{u}}\rangle_f) = 0 \tag{8}$$

$$\frac{\partial\phi\langle\overline{\mathbf{u}}\rangle_f}{\partial t} + \nabla\cdot(\phi\langle\overline{\mathbf{u}}\rangle_f\langle\overline{\mathbf{u}}\rangle_f) + \nabla\cdot(\phi\boldsymbol{\tau}^t) = -\frac{\phi}{\rho}\nabla\langle p^{\star}\rangle_f + \nabla\cdot(2(\nu+\nu_{t_\phi})\langle\overline{\mathbf{S}}\rangle) + \phi\mathbf{F}_f \tag{9}$$

$$\frac{\partial\phi\langle k\rangle_f}{\partial t} + \nabla\cdot(\phi\langle k\rangle_f\langle\overline{\mathbf{u}}\rangle_f) + \nabla\cdot(\phi\boldsymbol{\tau}^k) = \nabla\cdot\left(\left(\nu+\frac{\nu_{t_\phi}}{\tilde{\sigma}_k}\right)\nabla(\phi\langle k\rangle_f)\right) + 2\phi\nu_{t_\phi}\langle\overline{\mathbf{S}}\rangle_f : \langle\overline{\mathbf{S}}\rangle_f + \phi P_k - \phi\langle\epsilon\rangle_f \tag{10}$$

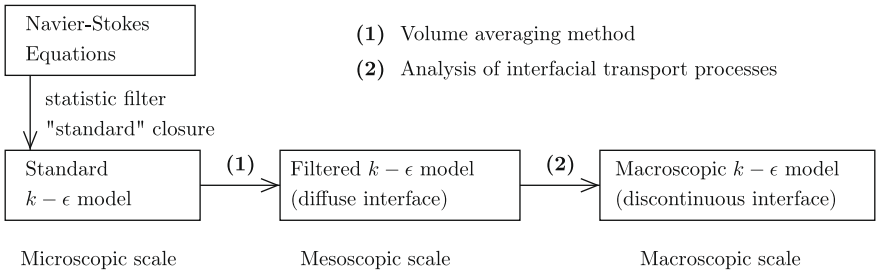

Fig. 3. Modeling approach.

$$\frac{\partial \phi\langle\epsilon\rangle_f}{\partial t} + \nabla\cdot(\phi\langle\epsilon\rangle_f\langle\overline{\mathbf{u}}\rangle_f) + \nabla\cdot(\phi\boldsymbol{\tau}^{\epsilon}) = \nabla\cdot\left(\left(\nu + \frac{\nu_{t_\phi}}{\tilde{\sigma}_\epsilon}\right)\nabla(\phi\langle\epsilon\rangle_f)\right) + \phi(2c_1\nu_{t_\phi}\langle\overline{\mathbf{S}}\rangle_f : \langle\overline{\mathbf{S}}\rangle_f - c_2\langle\epsilon\rangle_f)\frac{\langle\epsilon\rangle_f}{\langle k\rangle_f} + \phi\, P_\epsilon \quad (11)$$

except that, at this point, subfilter dispersion terms are still present. In the system (8)–(11), $\overline{\psi}$ denotes the statistic (or Reynolds) average of the quantity ψ, (c_1, c_2) are the two constants of the standard microscopic $k-\epsilon$ model whose values are respectively (1.44, 1.92) (Launder and Spalding, 1972), $(\tilde{\sigma_k}, \tilde{\sigma_\epsilon})$ are macroscopic turbulent Prandtl numbers, $p^{\star}$ is the modified pressure $(p^{\star} = \overline{p} + 2\rho k/3)$, $\langle\overline{\mathbf{S}}\rangle$ is the Reynolds- and volume-averaged deformation tensor:

$$\langle\overline{\mathbf{S}}\rangle \hat{=} \frac{1}{2}(\nabla\langle\overline{\mathbf{u}}\rangle + \nabla\langle\overline{\mathbf{u}}\rangle^T) \quad (12)$$

The three subfilter dispersion terms are defined by:

$$\boldsymbol{\tau}^t \hat{=} \frac{1}{\phi}(\langle\overline{\mathbf{u}}\overline{\mathbf{u}}\rangle - \phi\langle\overline{\mathbf{u}}\rangle_f\langle\overline{\mathbf{u}}\rangle_f) \quad (13)$$

$$\boldsymbol{\tau}^k \hat{=} \frac{1}{\phi}(\langle k\overline{\mathbf{u}}\rangle - \phi\langle k\rangle_f\langle\overline{\mathbf{u}}\rangle_f) \quad (14)$$

$$\boldsymbol{\tau}^{\epsilon} \hat{=} \frac{1}{\phi}(\langle\epsilon\overline{\mathbf{u}}\rangle - \phi\langle\epsilon\rangle_f\langle\overline{\mathbf{u}}\rangle_f) \quad (15)$$

In Eqs. (9)–(11), the presence of the porous matrix and the application of the volume average operator have brought out three additional source terms: the friction force $\mathbf{F}_f$ and the additional source terms P_k and P_ϵ. Their expression are given by:

$$\mathbf{F}_f = \frac{1}{\phi}\frac{1}{V}\int_{A_i}\left(-\frac{\tilde{p^{\star}}}{\rho}\mathbf{I} + \nu\nabla\tilde{\overline{\mathbf{u}}}\right)\cdot\mathbf{n}dS - \frac{\nu}{\phi}\nabla\phi\cdot\nabla\langle\overline{\mathbf{u}}\rangle_f \quad (16)$$

$$\phi P_k = 2\langle\nu_t\overline{\mathbf{S}} : \overline{\mathbf{S}}\rangle - 2\nu_{t_\phi}\phi\langle\overline{\mathbf{S}}\rangle_f : \langle\overline{\mathbf{S}}\rangle_f \quad (17)$$

$$\phi P_\epsilon = \left\langle(2c_1\nu_t\overline{\mathbf{S}} : \overline{\mathbf{S}} - c_2\epsilon)\frac{\epsilon}{k}\right\rangle - \phi\left(2c_1\nu_{t_\phi}\langle\overline{\mathbf{S}}\rangle_f : \langle\overline{\mathbf{S}}\rangle_f - c_2\langle\epsilon\rangle_f\right) \times\frac{\langle\epsilon\rangle_f}{\langle k\rangle_f} + \frac{1}{V}\int_{A_i}\nu\nabla\epsilon\cdot\mathbf{n}dS + \nabla\cdot\left(\left(\nu + \frac{\nu_{t_\phi}}{\tilde{\sigma}_\epsilon}\right)\frac{1}{V}\int_{A_i}\epsilon\mathbf{n}dS\right) \quad (18)$$

where A_i is the fluid–solid interfacial area and $\mathbf{n}$ is the unity normal vector oriented outward from the fluid into the solid phase. We recall that P_k and P_ϵ represent subfilter terms of production of $\langle k\rangle$ and $\langle\epsilon\rangle$ due to the application of the volume average operator, the presence of solids in the domain and the decomposition of the volume-averaged production terms in mesoscopic production terms (i.e. due to the mesoscopic velocity gradients) and subfilter production terms (see Eqs. (17) and (18)).

At the microscopic scale, the $k-\epsilon$ model is based on the turbulent viscosity concept, introduced by Boussinesq in 1877. The Reynolds stress tensor is expressed using the mean deformation tensor:

$$-\overline{\mathbf{u}'\mathbf{u}'} = 2\nu_t\overline{\mathbf{S}} - \frac{2}{3}k\mathbf{I} \quad (19)$$

The macroscopic turbulent viscosity ν_{t_ϕ}, which appears in the system (8)–(11), is the one introduced by Pedras and De Lemos (2001a) and defined by

$$\langle\nu_t\overline{\mathbf{S}}\rangle \hat{=} \nu_{t_\phi}\langle\overline{\mathbf{S}}\rangle \quad (20)$$

It allows to express the volume-averaged Reynolds stress tensor with the volume-averaged mean deformation tensor:

$$-\langle\overline{\mathbf{u}'\mathbf{u}'}\rangle = 2\nu_{t_\phi}\langle\overline{\mathbf{S}}\rangle - \frac{2}{3}\phi\langle k\rangle_f\mathbf{I} \quad (21)$$

Relation (21) can therefore be viewed as the expression of a macroscopic turbulent viscosity concept. To model the macroscopic turbulent viscosity, ν_{t_ϕ}, Nakayama and Kuwahara (1999) and Pedras and De Lemos (2001a) follow the modeling of the microscopic turbulent viscosity, ν_t, of the standard $k-\epsilon$ model and suggest:

$$\nu_{t_\phi} = C_\mu\frac{\langle k\rangle_f^2}{\langle\epsilon\rangle_f} \quad (22)$$

where C_μ is the constant of the standard microscopic $k-\epsilon$ model whose value is 0.09.

To close the system (8)–(11) at the mesoscopic scale, expressions for the three source terms ($\mathbf{F}_f, P_k$ and P_ϵ) and for the three dispersion terms ($\boldsymbol{\tau}^t, \boldsymbol{\tau}^k$ and $\boldsymbol{\tau}^{\epsilon}$) have to be specified. Since the physics is not the same in the entire domain, the domain is divided into three regions:

- The homogeneous free fluid region in which the porosity equals unity.
- The transition region which is characterized by a spatially varying porosity.
- The homogeneous porous region in which the porosity is constant, equals to ϕ_p.

3.1. Homogeneous free fluid region

In the free fluid region, since there is no solid, the porosity equals unity and the drag term $\mathbf{F}_f$ vanishes. Furthermore, the subfilter dispersion terms can be neglected if the filter length is sufficiently small compared to the scale of variation of the statistic averaged quantities, i.e. if $\langle\overline{\psi}\rangle \approx \overline{\psi}$. If this hypothesis is verified and since there is no solid, the two additional source terms P_k and P_ϵ vanish also in this region (see Eqs. (17) and (18)). Consequently, under this hypothesis, the system (8)–(11) reduces naturally to the standard $k-\epsilon$ model in the free fluid region, as expected.

3.2. Homogeneous porous region

In the homogeneous porous region, the modeling of the source terms $\mathbf{F}_f, P_k$ and P_ϵ is directly related to the structure of the porous medium. Some correlations are available in the literature to model them for different geometries: square (Nakayama and Kuwahara, 1999), circular (Pedras and De Lemos, 2001a) or elliptic (Pedras and De Lemos, 2001b) rods, channels and pipes (Chandesris et al., 2006). Regarding, the subfilter dispersion terms $\boldsymbol{\tau}^t, \boldsymbol{\tau}^k$ and $\boldsymbol{\tau}^{\epsilon}$, their influence is usually either supposed to be taken into account by the corresponding subfilter source terms $\mathbf{F}_f, P_k$ and P_ϵ (Pedras and De Lemos, 2001a), or simply neglected (Breugem and Boersma, 2005; Breugem et al., 2006). In fact, the subfilter dispersion terms might not be negligible. However, they appear in divergence operators and in the homogeneous porous region, far from interfaces with other media, the variations of the averaged quantities are very small (Nakayama and Kuwahara, 1999). Therefore, it seems reasonable to neglect the influence of these subfilter dispersion terms.

3.3. Transition region

In the transition region, the closure problem is more complex. The correlations determined for homogeneous porous media are *a priori* no longer valid and the resolution of the closure problem is not solved yet. As recalled in Section 2, one way to overcome this difficulty is to postulate the form of the closed equations and of the correlations corresponding to these closed equations. Then, from these choices, to deduce the different profiles of the parameters of the correlations by filtering microscopic $k-\epsilon$ simulations.

Finally, one must check that the profiles of these parameters are independent of the flow conditions. We will not perform such a study, because the specification of these profiles is not required at this point of the study. Furthermore, these profiles are directly related to the porous medium structure and we prefer to conduct a general study. Therefore, we only assume that the transition region is correctly described by considering that the different parameters of the correlations available in the literature to model $\mathbf{F}_f, P_k$ and P_ϵ vary continuously from their values in the homogeneous porous region to their values in the homogeneous free fluid region. We will then study the consequences of this choice.

Regarding the subfilter dispersion terms $\boldsymbol{\tau}^t, \boldsymbol{\tau}^k$ and $\boldsymbol{\tau}^\epsilon$, their influence might not be negligible since the variations of the averaged quantities are strong in this region. However, we do not know how to model them. Since they are null or negligible in the two homogeneous regions, we will assume that their influence in the transition region is directly taken into account through the variations of the parameters of the correlations of the three source terms $\mathbf{F}_f, P_k$ and P_ϵ. As a consequence, the subfilter dispersion terms will not appear directly in the remainder of the article.

Thus, at the mesoscopic scale of description, the flow is governed by a single system of Eqs. (8)–(11), valid in the entire domain. The parameters of the closure relations vary continuously from their value in one homogeneous region to their value in the other homogeneous region. Furthermore, in the two homogeneous regions, the system (8)–(11) can be simplified and reduces to the models classically used in these regions.

4. Jump conditions

The objective of this section is to derive the jump conditions that must be applied at the macroscopic scale (see Fig. 3). This derivation is based on the surface-excess theory of interfacial transport processes. However, this derivation is restricted to the particular geometry of a channel partially filled by a porous medium (see Fig. 1). Once the statistic and volumetric averages have been applied, the problem is one-dimensional in the direction normal to the interface (y-direction). From the continuity Eq. (9) and since the velocity vanishes at the upper wall, it comes that the y-component of the velocity is zero. Thus, at the mesoscopic scale, the set of Eqs. (8)–(11) reduces to:

$$0 = \underbrace{\frac{\partial}{\partial y}\left((\nu+\nu_{t_\phi})\frac{\partial\langle\overline{u}\rangle}{\partial y}\right)}_{f_\nu} - \underbrace{\frac{\phi}{\rho}\frac{\partial\langle p^\star\rangle_f}{\partial x}}_{f_p} + \underbrace{\phi\mathbf{F}_f}_{f_f} \tag{23}$$

$$0 = \underbrace{\frac{\partial}{\partial y}\left(\left(\nu+\frac{\nu_{t_\phi}}{\tilde{\sigma}_k}\right)\frac{\partial(\phi\langle k\rangle_f)}{\partial y}\right)}_{\mathrm{diff}_k} + \underbrace{2\nu_{t_\phi}\phi\langle\overline{\mathbf{S}}\rangle_f:\langle\overline{\mathbf{S}}\rangle_f}_{\mathrm{prodM}_k} + \underbrace{\phi P_k}_{\mathrm{prod}_k} - \underbrace{\phi\langle\epsilon\rangle_f}_{\mathrm{diss}_k} \tag{24}$$

$$0 = \underbrace{\frac{\partial}{\partial y}\left(\left(\nu+\frac{\nu_{t_\phi}}{\tilde{\sigma}_\epsilon}\right)\frac{\partial(\phi\langle\epsilon\rangle_f)}{\partial y}\right)}_{\mathrm{diff}_\epsilon} + \underbrace{2c_1\nu_{t_\phi}\phi\langle\overline{\mathbf{S}}\rangle_f:\langle\overline{\mathbf{S}}\rangle_f\frac{\langle\epsilon\rangle_f}{\langle k\rangle_f}}_{\mathrm{prodM}_\epsilon} - \underbrace{\phi c_2\frac{\langle\epsilon\rangle_f^2}{\langle k\rangle_f}}_{\mathrm{diss}_\epsilon} + \underbrace{\phi P_\epsilon}_{\mathrm{prod}_\epsilon} \tag{25}$$

where u represents the x-component of the velocity field. Since the pressure gradient is zero in the y-direction (projection of the momentum equation on the y-axis), it follows that the pressure gradient $d\langle p^\star\rangle_f/dx$ is a constant.

At the macroscopic scale, the domain is described by two homogeneous regions separated by a discontinuous interface. In the free fluid region, the flow is governed by the standard $k-\epsilon$ model ($\mathbf{F}_f, P_k$ and P_ϵ vanish) and in the homogeneous porous region by the macroscopic $k-\epsilon$ model where the parameters of the correlations for $\mathbf{F}_f, P_k$ and P_ϵ do not depend on the y-coordinate. These correlations depend only on macroscopic quantities and on the structure of the porous medium (see Table 1 for an example). They will be noted thereafter $\mathbf{F}_f^p, P_k^p$ and P_ϵ^p.

Table 1
Source terms for the macroscopic turbulence model of Nakayama and Kuwahara (1999).

P_k	ϵ_∞
P_ϵ	$c_2\ \epsilon_\infty^2/k_\infty$
	$\epsilon_\infty = 39\ \phi^2(1-\phi)^{5/2}\langle\overline{u}\rangle_f^3/d_p$ $k_\infty = 3.7(1-\phi)\phi^{3/2}\langle\overline{u}\rangle_f^2$

4.1. Momentum equation

In the study of interfacial processes, the jump conditions are obtained by integrating in the entire domain, the difference between the mesoscopic and the macroscopic equations governing the problem. The difference between the mesoscopic and the macroscopic momentum equations in the free fluid region (i.e. for $y > y_M$) is:

$$0 = \frac{\partial}{\partial y}\left((\nu+\nu_{t_\phi})\frac{\partial\langle\overline{u}\rangle}{\partial y}\right) - \frac{\partial}{\partial y}\left((\nu+\nu_{t_\phi})\frac{\partial U}{\partial y}\right) - \frac{(\phi(y)-1)}{\rho}\frac{d\langle p^\star\rangle_f}{dx} + (f_f(y)-0) \tag{26}$$

where U denotes the Reynolds- and volume-averaged velocity at the macroscopic scale and $f_f(y)$ is the friction force at the mesoscopic scale.

In the porous region, (i.e. for $y < y_M$), one gets:

$$0 = \frac{\partial}{\partial y}\left((\nu+\nu_{t_\phi})\frac{\partial\langle\overline{u}\rangle}{\partial y}\right) - \frac{\partial}{\partial y}\left((\nu+\nu_{t_\phi})\frac{\partial U}{\partial y}\right) - \frac{(\phi(y)-\phi_p)}{\rho}\frac{d\langle p^\star\rangle_f}{dx} + (f_f(y)-\phi_p\mathbf{F}_f^p) \tag{27}$$

Integrating Eq. (26) between y_M and H, where H is the height of the free fluid region, integrating Eq. (27) between $-\infty$ and y_M and then adding the corresponding equations, it comes, after integration of the viscous term:

$$0 = \left((\nu+\nu_{t_\phi})\frac{\partial\langle\overline{u}\rangle}{\partial y}\bigg|_H - (\nu+\nu_{t_\phi})\frac{\partial U}{\partial y}\bigg|_H\right) - \left((\nu+\nu_{t_\phi})\frac{\partial U}{\partial y}\bigg|_{y_M^+} - (\nu+\nu_{t_\phi})\frac{\partial U}{\partial y}\bigg|_{y_M^-}\right) - (f_p)^{EX} + (f_f)^{EX} \tag{28}$$

where

$$(f_f)^{EX} = \int_{-\infty}^{y_M}(f_f(y)-\phi_p\mathbf{F}_f^p)dy + \int_{y_M}^{H}(f_f(y)-0)dy \tag{29}$$

is the surface-excess force associated to the friction force and

$$(f_p)^{EX} = \left(\int_{-\infty}^{y_M}(\phi(y)-\phi_p)dy + \int_{y_M}^{H}(\phi(y)-1)dy\right)\frac{1}{\rho}\frac{d\langle p^\star\rangle_f}{dx} \tag{30}$$

$$= (\phi)^{EX}\frac{1}{\rho}\frac{d\langle p^\star\rangle_f}{dx} \tag{31}$$

is the surface-excess force associated to the pressure force.

By construction, the mesoscopic and macroscopic models are different in the interfacial transition region but they aim at being equivalent in the homogeneous regions. Therefore, the mesoscopic and macroscopic velocities should be equal in the homogeneous regions and the first term in the right-hand side of Eq. (28) should vanish. Thus, we obtain:

$$(\nu+\nu_{t_\phi})\frac{\partial U}{\partial y}\bigg|_{y_M^+}-(\nu+\nu_{t_\phi})\frac{\partial U}{\partial y}\bigg|_{y_M^-}=-(f_p)^{EX}+(f_f)^{EX} \tag{32}$$

This equation is the stress jump condition. Its form shows that the boundary condition associated to the momentum equation takes into account the whole diffusive flux, i.e. $(\nu+\nu_{t_\phi})\partial U/\partial y$. This shows in particular that the macroscopic turbulent viscosity must be introduced as was intuited by Silva and De Lemos (2003). Furthermore, the jump condition (32) is explicitly related to the pressure and friction surface-excess forces. Thus, the origin of the jump condition is linked to the fact that the pressure and friction forces are not correctly described by the macroscopic model in the transition region compared to the mesoscopic model. The jump condition is due to the existence of pressure and friction forces in the transition region that are not simple and are therefore not correctly described by the macroscopic equations. In this framework, Eq. (32) can simply be seen as a force balance integrated over the interfacial transition region.

At this stage of the analysis, the form of the stress jump condition has been derived and not postulated. Furthermore, the physical origin of the jump is clear. However, Eq. (32) still requires to be closed by making explicit or by evaluating $(f_f)^{EX}$ in terms of macroscopic variables. For the other excess quantity, $(f_p)^{EX}$, its value is given by Eq. (31).

4.2. k and ϵ transport equations

For the k and ϵ transport equations the method is similar and we get:

$$\left(\nu+\frac{\nu_{t_\phi}}{\tilde{\sigma}_k}\right)\frac{\partial \mathscr{K}}{\partial y}\bigg|_{y_M^+}-\left(\nu+\frac{\nu_{t_\phi}}{\tilde{\sigma}_k}\right)\frac{\partial \mathscr{K}}{\partial y}\bigg|_{y_M^-}=-(\mathrm{prodM}_k)^{EX}-(\mathrm{prod}_k)^{EX}+(\mathrm{diss}_k)^{EX} \tag{33}$$

$$\left(\nu+\frac{\nu_{t_\phi}}{\tilde{\sigma}_\epsilon}\right)\frac{\partial E}{\partial y}\bigg|_{y_M^+}-\left(\nu+\frac{\nu_{t_\phi}}{\tilde{\sigma}_\epsilon}\right)\frac{\partial E}{\partial y}\bigg|_{y_M^-}=-(\mathrm{prodM}_\epsilon)^{EX}-(\mathrm{prod}_\epsilon)^{EX}+(\mathrm{diss}_\epsilon)^{EX} \tag{34}$$

where $\mathscr{K}$ and E are respectively the volume average of the turbulent kinetic energy and of the dissipation at the macroscopic scale.

As was suggested by De Lemos and Silva (2006), see Eq. (2), a jump condition has to be taken into account for the diffusion flux of k. However, Eq. (34) shows that a similar jump condition must also be taken into account for the diffusion flux of ϵ. Furthermore, the jump conditions (33) and (34) are explicitly related to excess quantities of production and dissipation. Therefore, their physical origin is linked to the fact that in the transition region, production and dissipation terms of $\langle k\rangle$ and $\langle\epsilon\rangle$ are present but might not be correctly described by the macroscopic $k-\epsilon$ model compared to the mesoscopic $k-\epsilon$ model. Breugem and Boersma (2005) have shown that the flow near the permeable wall is dominated by relatively large-scale vortical structures, whose origin could come from a Kelvin–Helmholtz type of instability of the inflexional velocity profile. Therefore, the production and dissipation terms of $\langle k\rangle$ and $\langle\epsilon\rangle$ are important in the transition region. Furthermore, their nature is different from the one in the two homogeneous regions. Finally, to close relations (33) and (34), we still need to model or evaluate the related excess quantities in terms of macroscopic variables.

Thus, the surface-excess theory of interfacial transport processes allows to derive the *form* of the jump conditions that have to be imposed at a fluid/porous interface in a general and coherent way. However, these jump conditions are not closed at the macroscopic scale and the different excess quantities have to be modeled or evaluated to close the model.

Before studying these excess quantities, comments can be made regarding the boundary conditions that must be applied for the tangential component of the velocity $\langle\overline{u}\rangle$, $\langle k\rangle$ and $\langle\epsilon\rangle$. Indeed, the specification of these boundary conditions is mandatory to close the model at the macroscopic scale. In the laminar case, Chandesris and Jamet (2006) showed the continuity of the tangential component of the velocity using the method of matched asymptotic expansions. However, the surface-excess theory of interfacial transport processes does not give any information about these boundary conditions. Therefore, we will assume, as in previous studies (Lee and Howell, 1987; Silva and De Lemos, 2003; De Lemos, 2005), that these three quantities are continuous at the discontinuous interface.

5. Determination of the excess quantities

The objective of this section is to evaluate the different excess quantities that appear in the expressions for the boundary conditions (32)–(34). To perform this evaluation, we could use or perform microscopic $k-\epsilon$ simulations on different porous medium geometries. However, since Breugem and Boersma (2005) have performed two very comprehensive DNS for the particular geometry of a porous medium made of small cubes, we have chosen to use these DNS and this particular geometry to assess our model.

5.1. Geometry description

The geometry studied by Breugem and Boersma (2005) is recalled in Fig. 4. The simulations they realized are called DNS, because no turbulence model is introduced. However, two different levels of description of the interfacial transition region are studied. For the *DNS with cubes*, the flow field is resolved in the channel as well as in between the small cubes of the porous medium (see Fig. 4a). For the *DNS with continuum*, the cubes are replaced by an equivalent porous medium, whose properties (porosity, permeability and Forchheimer term) vary continuously in the transition region (see Fig. 4b).

The main characteristics of the geometry are the following. The cube size is $d_p=H/20$, where H is the height of the free fluid region. The distance between two cubes is equal to the size of the cube d_p. Consequently, the porosity of the porous medium is $\phi_p=0.875$. The bulk Reynolds number $Re_b=U_bH/\nu$, is fixed to 5500. Here, U_b is the bulk velocity in the channel region $(0<y<H)$.

For the DNS with continuum, Breugem and Boersma (2005) use the Darcy–Forchheimer expression to model the friction force:

$$f_f(y;\langle\overline{u}\rangle)=-\nu\frac{1+F(y;\langle\overline{u}\rangle)}{K(y)}\phi(y)\langle\overline{u}\rangle \tag{35}$$

with the Irmay correlation (Irmay, 1965) for the permeability:

$$K(y)=K(\phi(y))=C_K\frac{(1-(1-\phi(y))^{1/3})^3(1+(1-\phi(y))^{1/3})}{C_K(1-\phi(y))}d_p^2 \tag{36}$$

and the MacDonald correlation (MacDonald et al., 1979) for the Forchheimer term:

$$\frac{F(y;\langle\overline{u}\rangle)}{K(y)}=\frac{F(\phi(y);\langle\overline{u}\rangle)}{K(\phi(y))}=C_F\frac{1-\phi(y)}{\phi(y)^3}\frac{1}{d_p}\left(\frac{|\langle\overline{\mathbf{u}}\rangle|}{\nu}\right) \tag{37}$$

with $C_K=11.4$ and $C_F=0.4$. Regarding the porosity profile across the interfacial region, they use a fifth-order polynomial function that approximates the porosity profile obtained using the volume average operator. With the chosen volume average operator, the porosity profile vary in the region $-0.15<y/H<0$. In the homogeneous porous region, the friction force is of course evaluated by taking $\phi(y)=\phi_p$ in Eqs. (35)–(37).

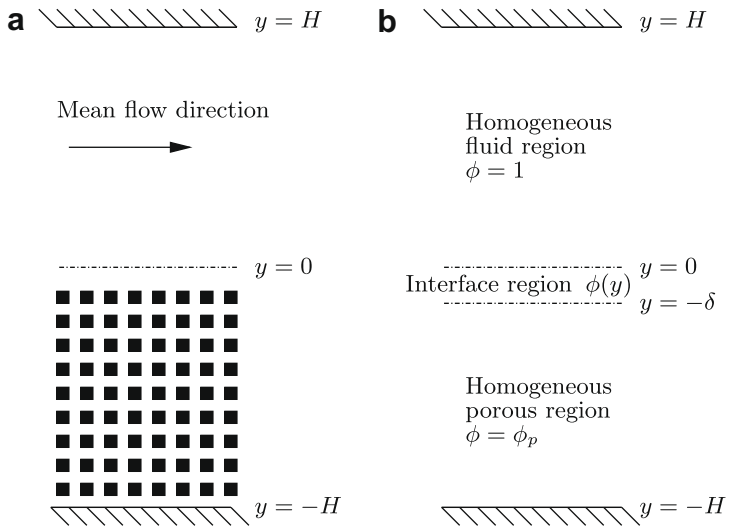

Fig. 4. Flow geometry: (a) DNS with cubes; and (b) DNS with a continuum approach.

5.2. Momentum equation

To close the momentum jump relation (32), we need to evaluate the friction surface-excess force, $(f_f)^{EX}$. For laminar flows, Chandesris and Jamet (2007) showed, using the method of matched asymptotic expansions, that this friction surface-excess force can be expressed in the following way, (we recall that the Forchheimer term is null for laminar flows):

$$(f_f)^{EX} = \left(\nu \frac{\phi}{K} u\right)^{EX} = \nu(y_{f_f} - y_M)\left(\frac{\phi_p}{K_p}\right)\langle u\rangle^{(0)}\Big|_{y_M} \tag{38}$$

where y_{f_f} is the center of gravity of the friction force (see Section 2 for the definition of the center of gravity of a quantity) and $\langle u\rangle^{(0)}$ is the velocity solution of the problem at order zero in the matched asymptotic expansions.

To get a similar result for turbulent flows, two modeling steps are necessary. First, one needs to check, using the matched asymptotic expansions, if a linearization similar to (38) is still valid for turbulent flows. We expect the result to be different because the friction force is no longer linear in velocity when the flow is turbulent (see Eqs. (35) and (37)). Second, the location of the center of gravity of the friction force y_{f_f} has to be reevaluated for turbulent flows. However, when the discontinuous interface, y_M, is located in y_{f_f}, the friction surface-excess force vanishes (see Eq. (38)). Therefore, for this particular location of the interface, one does not need to study the linearization of the friction surface-excess force to solve the problem. Consequently, we will only concentrate on the determination of the location of the center of gravity y_{f_f} when the flow is turbulent (Chandesris and Jamet, 2007; Breugem and Boersma, 2005).

Assuming that the velocities at the mesoscopic and macroscopic scales are almost identical in the transition region i.e. ($\langle\overline{u}\rangle \approx U$), we can substitute the unknown macroscopic velocity by the mesoscopic velocity in the expression for $(f_f)^{EX}$. Starting from Eq. (29) and using the modeling of the friction force given by Eq. (35), it comes:

$$\begin{aligned}(f_f)^{EX} \approx \nu \int_{-\infty}^{y_M} \left(\phi \frac{1+F(\phi;\langle\overline{u}\rangle)}{K}\langle\overline{u}\rangle - \phi_p \frac{1+F(\phi_p;\langle\overline{u}\rangle)}{K(\phi_p)}\ \langle\overline{u}\rangle\right) dy \\ + \nu \int_{y_M}^{H} \left(\phi \frac{1+F(\phi;\langle\overline{u}\rangle)}{K}\langle\overline{u}\rangle - 0\right) dy\end{aligned} \tag{39}$$

Using the mesoscopic velocity profile obtained by Breugem and Boersma (2005) and the expressions given in Section 5.1 for the porosity, permeability and Forchheimer profiles, we can deduce the value of y_M for which the right-hand side of Eq. (39) vanishes, which is therefore the location of the center of gravity y_{f_f}. We obtain $y_{f_f}/H = -0.0756$ for the DNS with cubes and $y_{f_f}/H = -0.0763$ for the DNS with continuum. These results are based on the assumption that the mesoscopic and macroscopic velocities are very close in the transition region. We will show in Section 6 that this is indeed the case, which validates *a posteriori* this assumption.

It is worth noticing that, for this geometry and for a laminar flow, Chandesris and Jamet (2007) show that $y_{f_f}/H = -0.08$. It means that, for this geometry, the centers of gravity of the friction force corresponding to laminar and turbulent flows are very close to each other. Since the determination of the center of gravity is much easier in the laminar case, one can directly use the results obtained for a laminar flow.

Regarding the pressure surface-excess force $(f_p)^{EX}$, its center of gravity is identical to the one of $(\phi)^{EX}$ (see Eq. (31)) and is therefore located in $y_{f_p}/H = -0.075$. This position is very close to that of the center of gravity of the turbulent friction force. Thus, we choose to locate the discontinuous interface at $y_M/H = -0.075$. For this location, the excess pressure force vanishes and the excess turbulent friction force is negligible ($y_{f_f}/H \approx -0.075$). Thus, one gets for the momentum jump relation (32):

$$(\nu + \nu_{t_\phi})\frac{\partial U}{\partial y}\Big|_{y_M^+} - (\nu + \nu_{t_\phi})\frac{\partial U}{\partial y}\Big|_{y_M^-} \approx 0 \tag{40}$$

5.3. k and ϵ transport equations

To evaluate the excess quantities present in the jump conditions (33) and (34), the profiles of the different production and dissipation terms at the mesoscopic scale are needed. However, these profiles are not provided by the DNS performed by Breugem and Boersma (2005). A microscopic $k-\epsilon$ simulation on the geometry of the Fig. 4a would be necessary to get them. In order to simplify the study, we make the hypothesis that the sum of the right-hand side of Eqs. (33) and (34) vanishes or is negligible when the interface is located at the center of gravity of the friction surface-excess force, in $y_M/H = y_{f_f}/H = -0.075$. We acknowledge that this hypothesis is strong and that it could be analyzed in more details,

however, as shown in Section 6, the results obtained with this hypothesis are very good.

6. Results and discussion of the model

In the free fluid region, the standard $k-\epsilon$ model is used. Since the bulk Reynolds number is moderate ($Re_b = 5500$), the standard $k-\epsilon$ model might not be the most appropriate. However, at this point, we do not wish to make the problem more complicated by using a low Reynolds $k-\epsilon$ model. Therefore, the standard wall function is applied at the upper wall. To ensure its validity, the first computational node is located in the logarithmic zone ($y^+ > 30$). However, since the Reynolds number is moderate, it implies that the size of the first computational cell is large. Thus, the mesh is refined far from the upper wall. The total number of cells used in the y-direction is 65.

In the homogeneous porous region, the porosity is equal to 0.875 and the values of $K(\phi_p)$ and $F(\phi_p)$ are deduced from Eqs. (36) and (37). For P_k^p and P_ϵ^p, we use the correlations suggested by Nakayama and Kuwahara (1999), which are adapted to a porous medium made of small cubes. These correlations are recalled in Table 1. The pressure gradient, $d\langle p^\star\rangle_f/dx$, is chosen such that $Re_b = 5500$.

The discontinuous interface is located at $y_M/H = y_{f_f}/H = -0.075$. As discussed in the previous section, for this particular position of the interface, the momentum, k and ϵ diffusion fluxes are supposed to be continuous. Therefore, no jump relation needs to be implemented for this case. The characteristics of the different simulations are listed in Table 2. The other Reynolds numbers characteristic of the study are $Re_\tau^t = u_\tau^t H/\nu, Re_\tau^p = u_\tau^p H/\nu$ and $Re_K = u_\tau^p\sqrt{K}/\nu$, where u_τ^t is the friction velocity at the upper wall and $u_\tau^p = ((\nu+\nu_t)\partial\langle u\rangle/\partial y)^{1/2}$ is the friction velocity at the "permeable wall" (the "permeable wall" is arbitrarily located in $y/H = 0$ by Breugem and Boersma (2005)).

6.1. Velocity

Fig. 5 shows the profiles of the Reynolds- and volume-averaged velocity of the present model along with the results of the DNS. The velocity obtained by Moser et al. (1999) for a channel with solid walls and for $Re_\tau = 360$ is also presented for comparison. The result of the $k-\epsilon$ model with the proposed boundary conditions is very good. Our model captures the main physical features of the flow. First, the strong increase in the Reynolds-shear stress at the permeable wall as compared to the solid wall is captured by the $k-\epsilon$ model (see Table 2 for the friction Reynolds numbers). However, we can see in this Table that, compared to the DNS with cubes, the model slightly overestimates the friction velocity at the upper wall (measured through Re_τ^t), whereas the friction velocity is slightly underestimated at the permeable wall. As a consequence of the dissymetry in the friction Reynolds number, the velocity profiles are strongly skewed, with the position of the maximum velocity well above the centerline of the channel. The position of the maximum velocity δ_w is given by (Breugem and Boersma (2005)):

$$\frac{\delta_w}{H} = \frac{(u_\tau^p)^2}{(u_\tau^p)^2 + (u_\tau^t)^2} \tag{41}$$

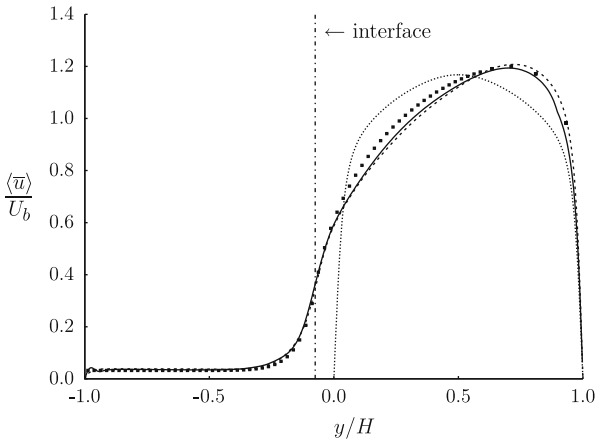

Fig. 5. Streamwise velocity profile, normalized by the bulk velocity U_b. —, DNS with cubes; - - -, DNS with continuum; ···, DNS with solid walls; symbol ■, present macroscopic $k-\epsilon$ model.

Its value is presented in Table 2. The $k-\epsilon$ model is able to recover the value obtained with the DNS with cubes with an error of 5% with only 65 points compared to the 9.6 10^7 points required for the DNS.

The velocity profiles in the transition region is also remarkably well captured by the $k-\epsilon$ model. Thus, the Reynolds- and volume-averaged velocity at the macroscopic scale (obtained with the present $k-\epsilon$ model) is almost identical to the Reynolds- and volume-averaged velocity at the mesoscopic scale (obtained by filtering the result of the DNS with cubes). This result supports the hypothesis made in Section 5.2 for the *a priori* estimation of the position of the center of gravity of $(f_f)^{EX}$.

6.2. Turbulent kinetic energy and dissipation

The profiles of the turbulent kinetic energy of the $k-\epsilon$ model, the DNS with cubes, the DNS with continuum and the DNS with solid walls are depicted in Fig. 6a. For the two DNS, the volume-averaged turbulent kinetic energy is obtained by taking the half sum of the streamwise, spanwise and wall-normal volume-averaged root-mean-square (rms) velocities. Fig. 6a shows that the $k-\epsilon$ model is able to recover the fact that the turbulent kinetic energy is higher close to the permeable wall than close to the solid wall. This effect is associated by Breugem and Boersma (2005) to the existence of relatively large-scale vortical structures close to the permeable wall, whereas the flow near the solid wall is characterized by elongated streaky structures.

The size of the peak of the turbulent kinetic energy close to the permeable wall is not exactly captured by the $k-\epsilon$ model. The position of the peak is also slightly shifted. This induces a slightly weaker value of the gradient of k along the channel height. However, the decrease of the turbulent kinetic energy in the porous medium is very well captured.

Fig. 6b shows the dissipation profile of the $k-\epsilon$ model. It shows a very strong peak at the interface. For comparison, the dissipation profile of the DNS with solid walls is also displayed, but the corresponding profiles for the DNS with cubes and with continuum are

Table 2
Characteristics of the different simulations.

	ϕ	Da	Re_b	Re_τ^p	Re_τ^t	Re_K	δ_w/H	Mesh points
DNS with cubes	0.875	3.4×10^{-4}	5500	669	394	12.4	0.742	9.6×10^7
DNS with cont.	0.875	3.4×10^{-4}	5500	726	409	13.5	0.759	1.57×10^7
Present $k-\epsilon$ model	0.875	3.4×10^{-4}	5500	642	417	11.8	0.703	65
DNS with solid walls			5640	360	360			

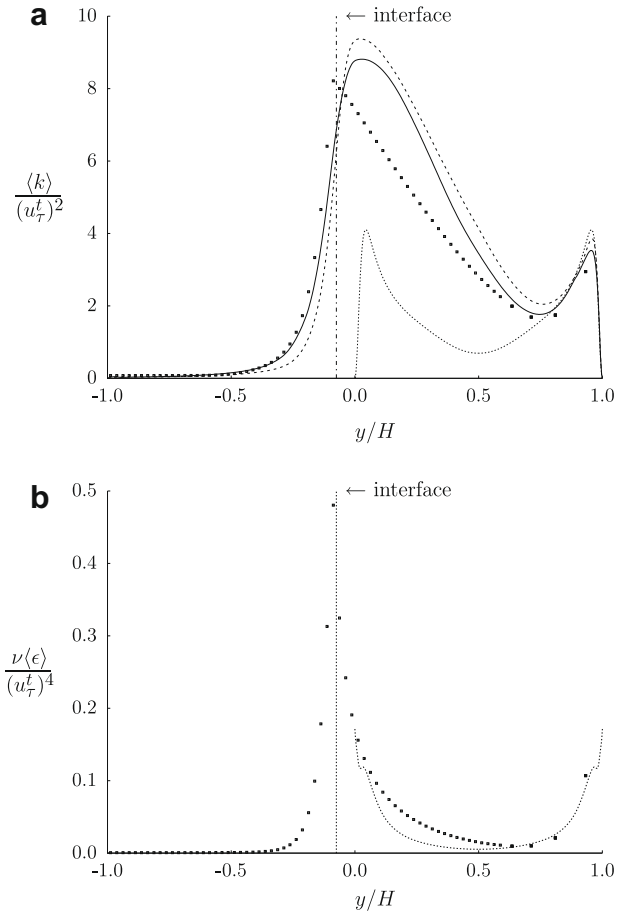

Fig. 6. Profiles of turbulent quantities. —, DNS with cubes; - - -, DNS with continuum; ···, DNS with solid walls; symbol ■, present macroscopic $k-\epsilon$ model. (a) Turbulent kinetic energy normalized by $(u_\tau^t)^2$, (b) dissipation normalized by $(u_\tau^t)^4/\nu$.

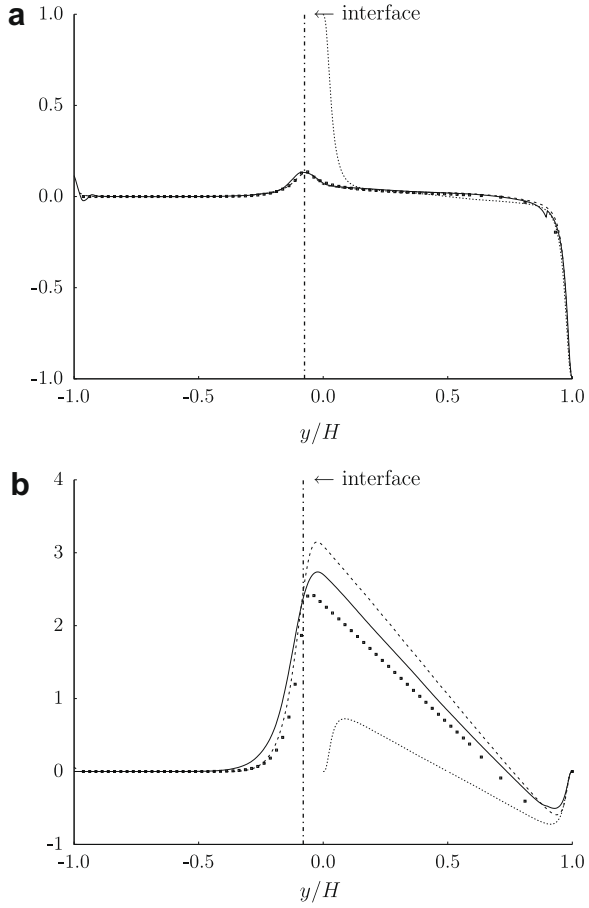

Fig. 7. Shear stress profiles, normalized by $(u_\tau^t)^2$. —, DNS with cubes; - - -, DNS with continuum; ···, DNS solid walls; ■, present macroscopic $k-\epsilon$ model. (a) Volume-averaged viscous shear stress; (b) volume-averaged Reynolds-shear stress.

unfortunately not available. The dissipation profile has a strong and narrow peak at the interface. However, it is worth noting that the characteristic length of this peak is smaller than the thickness of the filtered interfacial zone.

6.3. Shear stress

In the present macroscopic $k-\epsilon$ model, the volume-averaged Reynolds-shear stress $\langle\overline{u'w'}\rangle$ is modeled using the turbulent viscosity concept at the microscopic scale (Eq. (19)) and by introducing a macroscopic turbulent viscosity (Eq. (21)) which is evaluated using Eq. (22). Fig. 7 shows the viscous and volume-averaged Reynolds-shear stress profiles normalized by $(u_\tau^t)^2$ for the different simulations. The profiles of the viscous shear stress for the $k-\epsilon$ model and for the DNS compare very well. Regarding the Reynolds-shear stress, the $k-\epsilon$ model is able to capture the large increase reported in Breugem and Boersma (2005) close to the permeable wall. More precisely, the peak of the turbulent shear stress was overestimated by the DNS with continuum, whereas the present $k-\epsilon$ model slightly underestimates it. However, these differences are small compared to the profile of the DNS with solid walls.

6.4. Macroscopic turbulent viscosity

Since the volume-averaged Reynolds-shear stress is correctly evaluated by the present $k-\epsilon$ model, the model can be analyzed further by testing the macroscopic turbulent viscosity concept. For that purpose, we evaluate the ratio:

$$\frac{-\langle\overline{u'w'}\rangle}{d\langle\overline{u}\rangle/dy} \tag{42}$$

when the signs of the numerator and the denominator are identical for the DNS. This ratio corresponds to the definition of the macroscopic turbulent viscosity ν_{t_ϕ} (cf. Eq. (21)). In Fig. 8, this ratio is compared to the macroscopic turbulent viscosity profile obtained with the $k-\epsilon$ model, *i.e.* when the macroscopic turbulent viscosity concept is used in association with Eq. (22).

First, the macroscopic turbulent viscosity hypothesis is not verified in the porous region where $y/H \leqslant -0.5$ for the DNS with

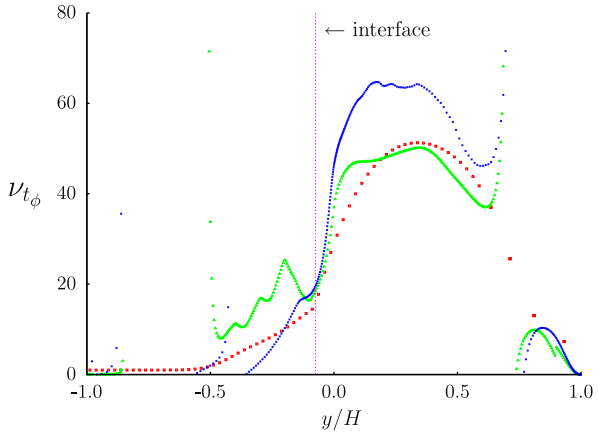

Fig. 8. Turbulent viscosity: hypothesis and profile. Symbol ▲, DNS with cubes; symbol ×, DNS with continuum; symbol ■, present macroscopic $k-\epsilon$ model.

cubes and the DNS with continuum, since the signs of the numerator and the denominator are not always identical. However, both the volume-averaged Reynolds-shear stress and the velocity gradient are negligible in this region as can be seen in Fig. 7. Therefore, the use of the macroscopic turbulent viscosity hypothesis has no consequence in the momentum equation in this region.

In the region where $-0.5 \leqslant y/H \leqslant 0$, the order of magnitude of the macroscopic turbulent viscosity is very well recovered by the model. It lies in between the profiles of the two DNS. In particular, the mean slope of the DNS with cubes seems to be captured by the present $k-\epsilon$ model.

In the free fluid region, where $y/H \geqslant 0$, the order of magnitude of the macroscopic turbulent viscosity is also very well recovered by the $k-\epsilon$ model and lies almost everywhere in between the profiles of the two DNS. Around $y/H = 0.7$, where the velocity gradient vanishes, the macroscopic turbulent viscosity hypothesis is not verified by the two DNS. Indeed, the volume-averaged Reynolds-shear stress and the velocity gradient do not vanish exactly at the same position and the ratio (42) tends to infinity. However, this discrepancy lies in a very small region where both the volume-averaged Reynolds-shear stress and the velocity gradient vanish. Therefore its influence should be negligible in the momentum equation.

6.5. Discussion

Our results show that, despite its simplicity, the $k-\epsilon$ model considered is able to capture the main physical features of the turbulent flow over a porous medium. In this section, we analyze the reasons that are at the origin of this very good behavior. We believe that the good results obtained with this model are due to the relative simplicity of the turbulence characteristics within the homogeneous porous region as well as within the porous region/ free fluid transition region.

Let us first discuss the turbulence characteristics of the flow within the porous region. At the microscopic scale, the flow in the pores is *a priori* very complex because of the source of turbulence at the solid boundaries and the impact of turbulent structures at these boundaries that tend to destroy the coherent structures of the turbulence. In the framework of the macroscopic $k-\epsilon$ model considered in this study, these complex phenomena are accounted for through two modeling hypotheses: (i) particular expressions for the specific subfilter production terms F_f^p, P_k^p and P_ϵ^p (see Table 1) and (ii) the use of a macroscopic turbulent viscosity hypothesis for the modeling of the volume-averaged Reynolds stress.

Far from the interface ($y/H \leqslant -0.5$), all the physical variables are almost constant. There is an equilibrium between the friction and the pressure forces and also between the production and the dissipation of turbulence. It is the study of the turbulence in this region that allows to determine the correlations for the specific subfilter production terms F_f^p, P_k^p and P_ϵ^p (see Nakayama and Kuwahara (1999); Pedras and De Lemos (2001a); Chandesris et al. (2006)). However, since the gradients are null or negligible in this region, the validity of the macroscopic turbulent viscosity hypothesis cannot be studied.

In the vicinity of the free boundary of the porous medium ($-0.5 \leqslant y/H \leqslant y_M/H$), large gradients of all the physical variables (u, k and ϵ) are present (see Figs. 5 and 6) over a region larger than the transition region (the transition region is characterized by a spatially varying porosity and lies therefore between $-0.15 \leqslant y/H \leqslant 0$). The macroscopic $k-\epsilon$ model captures the main physical features of the flow within this region, i.e. the strong decrease of the velocity, of the turbulent kinetic energy and of the turbulent dissipation. This exponential-like decrease is mostly due to the large velocity at the boundary that induces a large friction force and thus a strong decrease of the velocity and a large dissipation and thus a strong decrease of the turbulent kinetic energy. The most surprisingly good result is the linear decrease of the turbulent viscosity in the vicinity of the interfacial region, whose slope is very close to that given by the DNS results (see Fig. 8). This latter result shows the *a posteriori* validity of the macroscopic turbulent viscosity hypothesis (Eqs. (20) and (22)). These results mean that the main physical features within the porous region, even in the vicinity of the interfacial zone, are very well captured by the "standard" macroscopic $k-\epsilon$ model dedicated to homogeneous porous media.

Let us now discuss the physical features at the porous region/ free fluid transition region. Our results are based on the idea that the location of the centers of gravity of the interfacial production of $\langle k\rangle_f$ and $\langle \epsilon\rangle_f$ are the same as that of the friction force. With this simple assumption, we showed that the results obtained are very good compared to the reference DNS. It must be emphasized that the main criterion to validate the model is the velocity profile in the channel. Now, the turbulent and laminar velocity profiles are different only because of the presence of a turbulent viscosity in the turbulent case in the momentum equation. Therefore, once one can capture the laminar velocity profile, the key parameter to capture is the turbulent viscosity profile to get the correct turbulent velocity profile. Because of the simple turbulent viscosity hypothesis made, it is important to capture both the $\langle k\rangle_f$ and $\langle \epsilon\rangle_f$ profiles, in particular within the porous medium/free fluid interfacial region. The results presented in Fig. 6 show that the large value of the turbulent kinetic energy in the vicinity of the porous medium/free fluid interfacial zone is not primarily due to specific physical phenomena that develop within this interfacial region. Indeed, if that were the case, these specific physical phenomena should manifest themselves through specific terms in the equations that should be large within the interfacial zone or in its vicinity. Without these terms, the model should not provide accurate results. In the framework of our analysis of interfacial phenomena, these specific interfacial physical phenomena should appear through rather large values of the jump parameters. On the contrary, our results show that if these jump parameters are null, the main features of the flow are very well recovered. This means that the peak of the turbulent kinetic energy observed at the interface is only due to physical phenomena that are already accounted for in the standard free fluid and homogeneous porous standard $k-\epsilon$ models. For example, the production of turbulence in the porous region is due to two terms: a production associated to the volume averaged velocity gradient, prodM_k, and the subfilter production term, $\mathrm{prod}_k = \phi P_k$, (see Eq. (25)). These two terms take naturally high values in the porous region/free fluid transition region: the firt one, because the velocity gradient are large in this region; the second one, because the correlation determined for P_k varies like $(\langle \overline{u}\rangle_f)^3$ and the velocity takes large values in this region compared to the asymptotic velocity in the porous region. Therefore, the strong production of turbulence in the transition region is naturally taken into account by the homogeneous porous standard $k-\epsilon$ model.

Regarding the hypothesis made in Section 5.3 of neglecting the right-hand side of Eqs. (33) and (34) when the interface is located at the center of gravity of the friction surface-excess force, this hypothesis is not totally false given the good results obtained. However, it seems that the introduction of a small non-zero jump might improve the result by enhancing the value of the turbulent kinetic energy peak. However, given the good precision of the present results, this non-zero specific jump parameter would be a "first order" improvement. This means that the "zeroth order" solution corresponding to the main physical features of the flow, are very well captured by standard models.

This analysis tends to show that the complex turbulence characteristics of the flow at the interface between a porous domain

and a free fluid region as reported and described by Breugem and Boersma (2005) are actually already accounted for in the standard free fluid and homogeneous $k-\epsilon$ model. In particular, the present $k-\epsilon$ model is able to capture the effects of the large vortical structures that develop in the vicinity of the interface without resorting to specific terms. It means that no specific turbulence physics seems to develop at the free fluid/porous interface.

Based on a formal mathematical analogy of the momentum, $\langle k\rangle$ and $\langle\epsilon\rangle$ equations, De Lemos and Silva (2006) suggest to use not only the same form of the jump conditions for these three variables but also the same value of the jump coefficients. Our analysis shows that the jump conditions for these three variables should indeed involve the diffusion flux of these variables (see Eqs. (32)–(34)). Moreover, the physical origin of these jumps is now understood through the excess quantities involved in the expressions for these jumps. Furthermore, we have shown that these excess quantities vanish, or are negligible, for one particular position of the interface. This means that, for this particular position, all the jump coefficients are equal to zero. However, this does not necessarily mean that, for another interface position, the values of the jump coefficients are all equal; this would require further investigation. Indeed, since these excess quantities are related to different physical phenomena (pressure and friction forces, production and dissipation of $\langle k\rangle$ and $\langle\epsilon\rangle$), nothing indicates that they will behave similarly. The method of the matched asymptotic expansions could be used, as in Chandesris and Jamet (2007) to study this point. Indeed, the method should allow to express the excess quantities as functions of macroscopic variables and of excess quantities independent of the macroscopic variables. This would allow to determine whether the same jump coefficients can or cannot be used for these three jump conditions. The hypothesis that $U, \mathscr{K}$ and E are continuous at the interface could also be checked.

7. Conclusions

The objective of this article was to study the boundary conditions that must be imposed at a free-fluid/porous interface when the flow is turbulent and when $k-\epsilon$ turbulence models are used. The main idea is to derive these boundary conditions, starting from the knowledge of the flow at the microscopic scale and using a two-step up-scaling methodology.

First, this methodology has been applied to the standard $k-\epsilon$ turbulence model to derive in a coherent way the *form* of the jump conditions for the momentum, $\langle k\rangle$ and $\langle\epsilon\rangle$ diffusion fluxes (Eqs. (32)–(34)). The macroscopic turbulent viscosity appears naturally in these expressions. Furthermore, these jump conditions are explicitly related to excess quantities that need to be modeled or evaluated to close the model.

In a second step, these excess quantities have been evaluated for the particular geometry of a porous medium made of small cubes. Using an *a priori* estimation, we were able to determine the location of the interface for which the momentum jump vanishes. Assuming that the $\langle k\rangle$ and $\langle\epsilon\rangle$ fluxes jumps vanish also for this particular position of the interface, we were able to compare our model to the results of the DNS performed by Breugem and Boersma (2005). The results are very good and are obtained with a far less number of grid points, which is very important for engineering applications. This flow configuration is also interesting since it allows to test the macroscopic turbulent viscosity hypothesis and its modeling (Eq. (22)). Indeed, this hypothesis is often used for the study of turbulent flows in porous media, but had not been tested before. The comparison to the few available DNS results show that its use seems to be relevant for this type of configuration. This positive result is very encouraging in the effort to develop and validate macroscopic turbulence $k-\epsilon$ models.

Since the results have been obtained with the jump parameters being null and without resorting to specific terms, this study also shows that the characteristics of the flow at the interface are already accounted for in the standard free fluid and homogeneous porous $k-\epsilon$ model. No specific turbulence physics seems to develop at the free fluid/porous interface.

In a short term perspective, this research could be deepened by investigating in more details the different excess quantities appearing in the right-hand size of Eqs. (32)–(34). The excess quantities associated to the $\langle k\rangle$ and $\langle\epsilon\rangle$ diffusion-jump conditions should be studied to understand in more details their influence and their link to the excess quantities of the momentum jump condition (Chandesris and Jamet, 2007).

In a longer term perspective, this research could help to develop a logarithmic law dedicated to flow over porous media. This approach, used to simulate flows over rough wall and very interesting for engineering applications because the flow does not need to be computed in the porous region, is however still not mature for flows over porous media.

Acknowledgements

The authors want to warmly thank W.P. Breugem and B.J. Boersma for providing us the data of the DNS published in Breugem and Boersma (2005).

References

Beavers, G., Joseph, D., 1967. Boundary conditions at a naturally permeable wall. J. Fluid Mech. 30, 197–207.
Breugem, W., Boersma, B., 2005. Direct numerical simulations of turbulent flow over a permeable wall using a direct and a continuum approach. Phys. Fluids 17 (2), 025103.
Breugem, W., Boersma, B., Uittenbogaard, R., 2004. Direct numerical simulation of plane channel flow over a 3D cartesian grid of cubes. In: Reis, A.H., Miguel, A.F. (Eds.), Applications of Porous Media, Evora Geophysics Center, pp. 27–35.
Breugem, W., Boersma, B., Uittenbogaard, R., 2006. The influence of wall permeability on turbulent channel flow. J. Fluid Mech. 562, 35–72.
Chandesris, M., Jamet, D., 2006. Boundary conditions at a planar fluid–porous interface for a Poiseuille flow. Int. J. Heat Mass Transfer 49, 2137–2150.
Chandesris, M., Jamet, D., 2007. Boundary conditions at a fluid–porous interface: an a priori estimation of the stress jump coefficients. Int. J. Heat Mass Transfer 50, 3422–3436.
Chandesris, M., Jamet, D., in press. Jump conditions and surface-excess quantities at a fluid/porous interface: a multi-scale approach. Trans. Porous Media, doi:10.1007/s11242-08-9302-0.
Chandesris, M., Serre, G., Sagaut, P., 2006. A macroscopic turbulence model for flow in porous media suited for channel, pipe and rod bundle flows. Int. J. Heat Mass Transfer 49, 2739–2750.
De Lemos, M., 2005. Turbulent kinetic energy distribution across the interface between a porous and a clear region. Int. Commun. Heat Mass Transfer 32, 107–115.
De Lemos, M., Pedras, M., 2000. Simulation of turbulent flow through hybrid porous medium – clear fluid domains. In: Proceedings of the ASME Heat Transfer Division, vol. 5, pp. 113–122.
De Lemos, M., Silva, R., 2006. Turbulent flow over a layer of a highly permeable medium simulated with a diffusion-jump model for the interface. Int. J. Heat Mass Transfer 49, 546–556.
Edwards, D., Brenner, H., Wasan, D., 1991. Interfacial Transport Processes and Rheology. Butterworth-Heinemann.
Finnigan, J., 2000. Turbulence in plant canopies. Ann. Rev. Fluid Mech. 32, 519–571.
Gray, W., 1975. A derivation of the fluid equations for multi-phase transport. Chem. Eng. Sci. 30, 229–233.
Irmay, S., 1965. Modèles théoriques d'écoulement dans les corps poreux. Bull. Rilem. 29, 37–43.
Launder, B., Spalding, D., 1972. Mathematical Models of Turbulence. Academic Press, London.
Lee, K., Howell, J., 1987. Forced convective and radiative transfer within a highly porous layer exposed to a turbulent external flow field. In: Proceedings of the 1987 ASME-JSME Thermal Engineering Joint Conference, vol. 2, pp. 377–386.
MacDonald, I., El-Sayed, M., Mow, K., Dullien, F., 1979. Flow through porous media: the Ergun equation revisited. J. Fluid Mech. 18, 199–208.
Moser, R., Kim, J., Mansour, N., 1999. Direct numerical simulation of channel flow up to $Re_\tau = 590$. Phys. Fluid 4 (11), 943–945.
Nakayama, A., Kuwahara, F., 1999. A macroscopic turbulence model for flow in a porous medium. J. Fluid Eng. 121, 427–433.

Neale, G., Nader, W., 1974. Practical significance of Brinkman's extension of Darcy's law: coupled parallel flows within a channel and a bounding porous medium. Can. J. Chem. Eng. 52, 475–478.

Ochoa-Tapia, J., Whitaker, S., 1995a. Momentum transfer at the boundary between a porous medium and a homogeneous fluid – I. Theoretical development. Int. J. Heat Mass Transfer 38 (14), 2635–2646.

Ochoa-Tapia, J., Whitaker, S., 1995b. Momentum transfer at the boundary between a porous medium and a homogeneous fluid – II. Comparison with experiment. Int. J. Heat Mass Transfer 38 (14), 2647–2655.

Pedras, M., De Lemos, M., 2001a. Macroscopic turbulence modeling for incompressible flow through undeformable porous media. Int. J. Heat Mass Transfer 44, 1081–1093.

Pedras, M., De Lemos, M., 2001b. On the mathematical description and simulation of turbulent flow in a porous medium formed by an array of elliptic rods. J. Fluid Eng. 123, 941–947.

Pinson, F., Gregoire, O., Simonin, O., 2007. $k-\epsilon$ macro-scale modeling of turbulence based on a two scale analysis in porous media. Int. J. Heat Fluid Flow 27, 955–966.

Silva, R., De Lemos, M., 2003. Turbulent flow in a channel occupied by a porous layer considering the stress jump at the interface. Int. J. Heat Mass Transfer 46, 5113–5121.

Slattery, J., 1972. Momentum, Energy and Mass Transfer in Continua. McGraw-Hill, New York.

Uittenbogaard, R., 2003. Modeling turbulence in vegetated aquatic flows. In: Riparian Forest Vegetated Channels, Workshop Trento, Italy, pp. 1–17.

Watanabe, T., 2004. Large-eddy simulation of coherent turbulence structures associated with scalar ramps over plant canopies. Boundary-layer Meteorol. 112, 307–341.

Whitaker, S., 1969. Advances in theory of fluid motion in porous media. Ind. Eng. Chem. 61, 14–28.

Whitaker, S., 1999. The Method of Volume Averaging. Kluwer Academic Publishers.

Zhu, J., Kuznetsov, A., 2005. Forced convection in a composite parallel plate channel: modeling the effect of interface roughness and turbulence utilizing a k-eps model. Int. Commun. Heat Mass Transfer 32, 10–18.

Zwillinger, D., 1989. Handbook of Differential Equations. Academic Press, Boston.